Geophysical Journal International

Geophys. J. Int. (2015) **202,** 1613–1626 doi: 10.1093/gji/ggv247
GJI Marine geosciences and applied geophysics

The imprint of hydro-mechanics of fractures in periodic pumping tests

C. Vinci,[1,2] H. Steeb[1] and J. Renner[2]

[1] *Continuum Mechanics, Ruhr-University Bochum, D-44780 Bochum, Germany. E-mail: vinci@lkm.rub.de*
[2] *Experimental Geophysics, Ruhr-University Bochum, D-44780 Bochum, Germany*

Accepted 2015 June 8. Received 2015 May 19; in original form 2014 November 28

SUMMARY

Modelling of pressure transients recorded in wells allows for characterization of reservoirs surrounding the well. Simulation of pressure transients furthermore permits sensitivity studies for individual model parameters. We numerically simulated pumping tests in a vertical well intersecting a single horizontal fracture to evaluate the diagnostic potential of periodic pumping procedures for subsurface characterization. The pressure responses in the pumping and monitoring wells were analysed with respect to their sensitivity to geometrical and hydraulic properties of the fracture and of the surrounding rock material. We focused on interference analysis that for periodic pumping tests reduces to a consideration of amplitude ratio and phase shift between pressure transients recorded at an injection well and monitoring points. Fluid flow in the deformable fracture was modelled employing (1) a hybrid-dimensional hydro-mechanically coupled approach and (2) an uncoupled-diffusion equation. Results of both approaches were compared to quantify the effects of hydro-mechanical coupling. While in the uncoupled-diffusion approach a bulk storage capacity value is prescribed for the fracture, storage capacity is implicitly accounted for by the coupling in the hybrid-dimensional approach. Results reveal that hydro-mechanical coupling strongly affects the pressure transient at the pumping well and the monitoring points. Asymmetry of the pressure profiles between injection and production phases at the injection point is a peculiar characteristic of the hydro-mechanical results and is related to changes in fracture permeability with fluid pressure caused by fracture deformation. Further hydro-mechanical effects, such as reverse-pressure response, occur at monitoring points along the fracture domain, in particular at positions in the conduit where the contribution of diffusive pressure propagation remains small, that is, at monitoring distances large compared to classic scaling for penetration depth using hydraulic diffusivity. During periodic pumping tests the reverse response is potentially triggered various times within one period and thus chances to unequivocally recognize this effect are largely enhanced in comparison to conventional pulse or step testing procedures. The standard scaling relation for diffusion processes, often employed in the analysis of induced seismicity, has limited applicability to deformable fractures.

Key words: Numerical solutions; Fourier analysis; Permeability and porosity; Plasticity, diffusion, and creep; Fracture and flow.

1 INTRODUCTION

Pumping tests in boreholes are the primary tool for hydraulic characterization of subsurface reservoirs (e.g. Matthews & Russell 1967; Fetter 2001). Understanding fluid transport and the related transport of solutes, suspended solids and heat constitutes a crucial prerequisite for management of water resources, exploitation of oil and gas reservoirs, provision of geothermal energy from deep, the so-called petrothermal reservoirs, and underground disposal of gaseous or liquid waste. The principal strategy of pumping tests employs perturbations of the reservoir's current state by producing fluid from it or injecting fluid into it. The response of the reservoir documents itself in pressure transients recorded either in the pumping well itself or in nearby monitoring wells even long beyond the actual pumping operation. The pressure transients are the result of hydraulic and mechanical processes whose balance depends on various geometrical and material properties of the rock surrounding the wells. The pumping protocol also strongly affects to which extent processes are activated.

For more than half a century, the analysis has strongly relied on comparing transients recorded during and after phases of pumping with constant flow rate (conventional pulse or step testing,

e.g. Johnson *et al.* 1966; Kamal & Brigham 1975; Stegemeier 1982) to the results of analytical (or numerical) forward calculations for subsurface models representing idealized albeit evermore complex scenarios (e.g. James & Butler 1997; Bruggeman 1999). Characteristic plots of pressure and/or pressure derivative versus the natural logarithm of time allow the operator to readily infer aspects such as the flow regime (linear versus radial) or reservoir boundaries (infinite versus pressure or flow boundaries). The practitioner often settles for the determination of effective transport and storage properties of a reservoir or its components with the help of such type of curves in the time domain (Gringarten *et al.* 1975). Yet, from a fundamental science perspective the overarching goal of pumping tests is to constrain the reservoir's transfer or response function, formulated in the frequency space. Knowing the transfer function namely allows one to predict the reservoir response to pumping protocols different from the one applied during the testing (e.g. Krauss 1974; Marschall & Barczewski 1989), by convolution of the transfer function with the input function of interest.

In theory, the entire transfer function of a linear hydraulic system, that is, a system for which the superposition principle holds for several coeval perturbations, can be determined from a single perturbation (delta-like pulse or step-function). In practice, however, the amplitude spectrum exhibits limited reliability for small and large frequencies beyond the limitation on band width by maximum and minimum frequency resulting from sampling rate and experimental duration, respectively. High-frequency content is typically biased by the finite rise time of the real step or pulse. At intermediate and low frequencies, environmental and instrumental noise reduce the accuracy of the transfer function significantly. Marschall & Barczewski (1989) proposed to perform several pumping tests with varying perturbations to improve the resolution of the transfer function. Alternatively, the transfer function can be successively determined from periodic pumping tests (e.g. Black & Kipp 1981; Rasmussen *et al.* 2003; Renner & Messar 2006; Becker & Guiltinan 2010; Cardiff *et al.* 2013; Guiltinan & Becker 2015). Periodic signals permit massive filtering as long as the assumption of linearity is justified and environmental sources do not operate on the actively excited frequency. The analysis of periodic excitations in turn provides a unique opportunity for identifying non-linearity by amplitude variation.

Non-harmonic periodic signals excite more than a single frequency. Together with the main frequency such overtones, that is, signal components at a higher than the excitation frequency, provide the opportunity to constrain sections of the transfer function from a single test (e.g. Fokker *et al.* 2013; Renner & Messar 2006, fig. 3a and table 1). In addition, experimental observations can be easily extended by observations for natural periodic excitations (tides, seasons) once analysing the problem in frequency space (e.g. Davis & Becker 2004). Finally, periodic excitations are technically easy to perform and involve relatively smaller fluid volumes compared to step tests notably also allowing for zero net balance of fluid volume alleviating the storage infrastructure at the surface.

The increasing uncertainty of the transients recorded towards the end of conventional pumping tests employing constant flow rate poses a significant problem since the timescales of testing are typically much shorter than the timescales of subsequent reservoir operation such that predictions on long-term reservoir behaviour (whether in freshwater supply, hydrocarbon production, or geothermal energy provision) inevitably require extrapolation of the transfer function towards low frequencies. The analysis of periodic tests requires—as a rule of thumb—a minimum of three full periods. The apparent extra time invested in periodic testing in comparison to classical single-pulse testing, the period and the test duration constitute the longest time for which the transfer function can be constrained, respectively, is in practice offset by the much smaller uncertainty of the constraint on the transfer function achieved by filtering. Obviously, quality of extrapolation will be affected by the resolution of a transfer function and the understanding of the contributors to the investigated range of frequencies.

Numerical simulations of pressure transients can be used as a predictive tool that permits systematic studies of the sensitivity of flow characteristics to various geometrical properties and material parameters. The amount of work previously done in this direction is humongous (e.g. do Nascimento *et al.* 2005; Murdoch & Germanovich 2006; Cappa *et al.* 2008; Slack *et al.* 2013) and we name here only a few studies that bear close relation to our work. Pulse tests were numerically modelled to fit field data and allow for mechanical and hydraulic characterization of fractured rock domains (Cappa *et al.* 2008). Furthermore, some previous numerical analyses accounted for hydro-mechanical coupling of fluid pressure with solid deformations. Pressure-sensitive media, that is, media whose properties, such as transmissivity, are altered by fluid pressure variations, were modelled to gain an improved understanding of pressure transients recorded during pumping tests in wells (e.g. Murdoch & Germanovich 2006; Vasco & Minkoff 2009; Ortiz *et al.* 2011; Berg *et al.* 2014). In this work, periodic pumping tests were numerically modelled with the particular aim to understand the implications of hydro-mechanical coupling for the pressure transient observed in wells intersecting a planar hydraulic conduit, such as a joint, fracture, or fault.

Counterintuitive, pressure excursions in monitoring wells opposite to the pressure development in the pumping well constitute a prominent evidence of the importance of hydro-mechanical effects. These observations were historically addressed as 'reverse-pressure response' (Wolff 1970) and this terminology has later been used by Slack *et al.* (2013) and Gellasch *et al.* (2014). We will therefore abandon the term 'inverse response' previously used by us (Vinci *et al.* 2014a) unaware of the already established terminology. The reverse response to pumping occurs only when flux at the injection well is changed. During non-harmonic periodic pumping the reverse response is potentially triggered various times during a period and thus chances to unequivocally recognize this effect are largely enhanced.

In this study, synthetic data are produced employing two different models that describe the induced fluid flow. The hybrid-dimensional approach (Vinci *et al.* 2014a) is used to account for hydro-mechanical coupling. This method relies on basic conservation laws and does not introduce *a priori* assumptions on the fracture-storage capacity. We analyse the limitations of introducing the concept of storage capacity as a macroscopic, effective property of the fracture (e.g. Narasimhan 2006; Mavko *et al.* 2009; Murdoch & Germanovich 2012) by comparing the fully coupled results to numerical solutions of simple diffusion equations. Pressure transients are first qualitatively analysed in the time domain then quantitatively in the frequency domain relying on fast Fourier transformation (FFT). With the aim to estimate equivalent hydraulic parameters in mind, the sensitivity of the pressure transients to geometrical properties and material parameters is investigated for both modelling approaches.

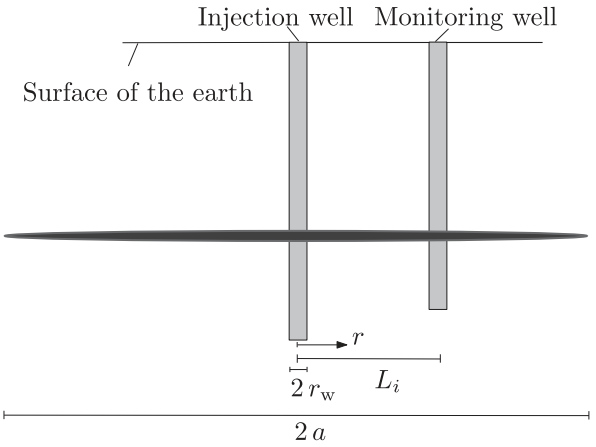

Figure 1. Analysed configuration: injection well (with radius r_w) and monitoring wells (at distances $5 < L_i < 550$ m) intersecting a single ellipsoidal fracture of length $2a$.

2 BACKGROUND AND MODELLING APPROACHES

2.1 Configuration of the wells and the fracture

Pumping procedures were investigated involving periodic injection of fluid into and production from a vertical well with radius r_w. Pressure was monitored in the pumping well and at distances $L = 5$–550 m from the injection point (Fig. 1). All boreholes were assumed to intersect a single horizontal ellipsoidal fracture of half length a, where $a \gg r_w$, through which fluid flow is induced, a conceptual model close to the one investigated by Murdoch & Germanovich (2006). The elliptical shape of the fracture is determined by its initial aperture at the pumping well, $\delta_0 = \delta(r = r_w, t_0)$, at time t_0 and the fracture half length a. The aspect ratio of the fracture is defined as $2a/\delta_0$. The numerical simulations were based on a general continuum model (Vinci *et al.* 2014b) in which the material surrounding the fracture was considered homogeneous and poro-elastic (Biot 1941). Yet, in the calculations to be presented here fluid mass exchange between the fracture and the surrounding rock, that is, leak-off, was 'inhibited' by assigning an intrinsic permeability of $k^s = 10^{-22}$ m^2 to the porous material. This low rock permeability was used to isolate effects induced by pressure-transport phenomena associated with the fracture, for example, diffusion or hydro-mechanical coupling effects. A periodic fluid-flow transient, consisting of a succession of injection, no-pumping, production, and no-pumping, was applied at the pumping well with periods $T =$ 37, 370, and 3700 s. The choice of material parameters, geometrical properties, and injection boundary conditions (Table 1) was based on the fitting of field data performed by Vinci *et al.* (2014a).

Additional simulations were performed to study the sensitivity of the reverse response to initial fracture aperture δ_0 and to the rock's drained bulk modulus K_d. For these calculations, we altered the boundary condition at the pumping well and used a step in pressure at the injection well to $p = 20$ kPa instead of the periodic flow-rate variations. The switch to a pressure boundary condition facilitates the comparison of pressure profiles for different parameters. For identical pressure values at the injection well, the transient behaviour of the pressure along the fracture obtained using different geometrical or material properties can be easily compared, in particular the magnitude and duration of the reverse response to pumping.

2.2 Modelling

2.2.1 Hybrid-dimensional approach

The hydro-mechanical problem of fluid injection in a deformable conduit is accounted for by a hybrid-dimensional approach. A fully coupled set of equations was previously derived by us from basic conservation laws for the specific heterogeneity, a horizontal fracture modelled as an ellipsoid (Vinci *et al.* 2014a,b), to interpret and analyse data records obtained during field tests (Renner & Messar 2006). We showed that this approach provides numerical approximations that are very similar to Biot's equations when used to model a poro-elastic slit in a poro-elastic matrix, but exhibit the advantage to efficiently account for large aspect ratio geometries.

Fluid flow along the fracture is addressed as a one-dimensional axisymmetric process with the governing equation

$$\frac{\partial p}{\partial t} + \frac{1}{12\,\eta^{fR}\,r}\,\frac{\partial}{\partial r}\left(-\frac{r\,\delta^2}{\beta_f}\,\frac{\partial p}{\partial r}\right) - \left(\frac{\delta}{12\,\eta^{fR}\,\beta_f}\,\frac{\partial \delta}{\partial r}\right)\frac{\partial p}{\partial r} - \frac{\delta^2}{12\,\eta^{fR}}\left(\frac{\partial p}{\partial r}\right)^2 = -\frac{1}{\beta_f\,\delta}\,\frac{\partial \delta}{\partial t} + q_L, \quad (1)$$

were $\delta(r, t)$ represents the local spatial and time-dependent aperture of the deformable fracture, η^{fR} is the effective fluid viscosity, $\beta_f = 1/K^f$ is the compressibility of the fluid and the source/sink term q_L accounts for leak-off. The governing eq. (1) was derived imposing equilibrium conditions in the fluid phase with respect to a deformable inclusion surrounded by a 2-D axisymmetric domain

Table 1. Parameters used for the simulation of periodic pumping tests.

Periodic pumping				
Pumping	T	=	370 s	
	$\hat{q}$	=	$\pm 4 \times 10^{-4}$ m^3 s^{-1}	
Fracture	a	=	1000 m	
	δ_0	=	640 μm	
Surrounding rock	K^s	=	14 GPa	grain
(hybrid-dimensional, eq. 1)	K_d	=	1.4 GPa	skeleton
	G	=	0.65 GPa	skeleton
	K^f	=	2.2 GPa	fluid
	ν	=	$(3K_d - 2G)/2(3K_d + G)$	skeleton
	ϕ_0	=	0.02	
	k^s	=	10^{-22} m^2	
Storage multiplier	α_s	=	10^5	
(uncoupled-diffusion, eq. 10)				

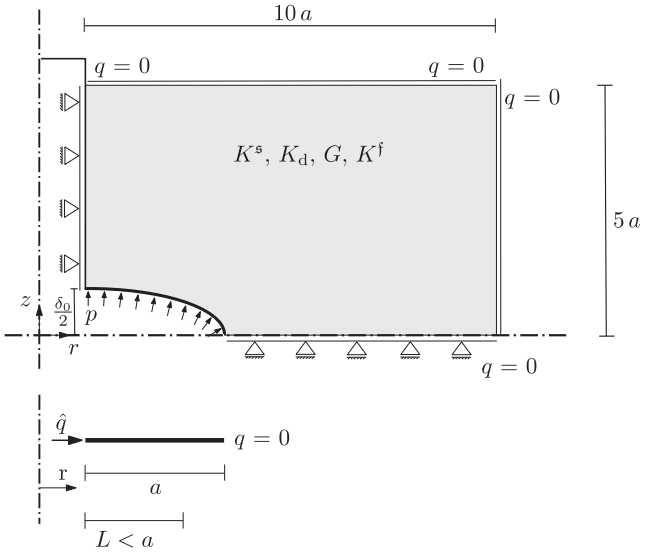

Figure 2. Initial geometry and initial-boundary-value problem of the fracture and the surrounding rock material (axial symmetry with respect to the vertical axis and symmetry with respect to the horizontal axis are exploited). In the framework of the hybrid-dimensional approach a 2-D axisymmetric poro-elastic domain is modelled while the fracture domain is represented as a 1-D axisymmetric domain. Leak-off of fluid between the fracture domain and the rock matrix is essentially inhibited using a low permeability $k^{\mathfrak{s}} = 10^{-22}$ m^2.

representing the rock matrix (Fig. 2; see also Vinci *et al.* 2014a,b) in which mechanical deformation as well as fluid flow are modelled by the standard poro-elastic equations (Biot 1941). Neither permeability nor storage capacity or closely related fracture stiffness are explicit parameters in the hybrid-dimensional approach. The latter are rather a result of the coupling between fluid pressure and solid deformation. Changes in fracture aperture are related to the pressure distribution, $\delta_{p(r,\,t)}$ (e.g. Sneddon 1995). For constant pressure, p_0, along the fracture, its stiffness (e.g. Valkó & Economides 1995) is simply

$$S_{\mathrm{F},0} = \frac{\partial \delta}{\partial p_0} = \frac{2\,a(1-\nu)}{\pi\, G}\,, \tag{2}$$

where G and ν denote shear modulus and Poisson's ratio, respectively. The assumption of a constant pressure along a fracture of finite length may be well justified for the intermediate to long timescales of pumping tests when the fracture simply extends the actual interface between pumped fluid and matrix (e.g. Ortiz *et al.* 2013) but the focus of the current study is transients in the fracture (early-time behaviour in the terminology of Weir 1999). In certain cases, the integral relation between aperture and pressure distribution may have a serial representation in terms of average pressure along the fracture, $\bar{p}$, in which stiffness $\partial\delta/\partial\bar{p}$ constitutes the weighting of the linear term. Here, instead of elaborating on such approximations or explicitly solving the Sneddon integral, fracture deformation is numerically calculated by means of the linear elastic constitutive material law in the poro-elastic equations (see Vinci *et al.* 2014a).

An approach that relies on the assumption of an ellipsoidal fracture geometry probably has limitations regarding mechanically closed fractures. The fracture stiffness is related to the sensitivity of deformations to variations in fluid pressure ($\partial\delta/\partial\bar{p}$) only where the fracture is mechanically open. In regions where the fracture is mechanically closed, that is, where asperities come into contact, the fracture stiffness is related to the elastic parameters of the material composing the asperities. Here we refrain from employing a more elaborate approach that accounts for both contributions to stiffness (e.g. Murdoch & Germanovich 2006) because our focus is on hydromechanics and we use the simplest model that allows us to study the basic effects. Nevertheless, our investigation intends to include mechanically closed fractures by employing rather high elasticity moduli for the surrounding rock (Table 2a and c), to indirectly account for the enhancement of stiffness by asperities.

The set of governing equations leading to eq. (1) and the poro-elastic equations (see Vinci *et al.* 2014a) are complemented by the boundary conditions for the fluid pressure and flux, the solid displacement and the total stress $\mathbf{T}$. On the boundaries of the 1-D axisymmetric domain a flux boundary condition $q(r_{\mathrm{w}}, t) = \hat{q}$ and a no-flux boundary condition $q(a, t) = 0$ are applied at the injection point and the fracture tip, respectively (Fig. 2); the fluid pressure $p(r, t)$ acts on the fracture surface of the porous rock domain ($\mathbf{T} = p\,\mathbf{n}$ and $p_{\mathrm{matrix}} = p$, where $\mathbf{n}$ is the unit vector normal to the fracture surface and p_{matrix} is the fluid pressure in the rock matrix), and the displacement of the porous matrix is coupled to the aperture of the fracture (Fig. 2), *cf.* $\delta(r, t)$ in eq. (1). At the boundaries of the 2-D axisymmetric domain, representing the far field, undrained boundary conditions are applied and, according to vertical symmetry, vertical displacement is inhibited at the lower edge (Fig. 2). The finite dimensions of the monitoring boreholes are not simulated in the 1-D axisymmetric domain and, therefore, borehole storage effects are not modelled. Pressure transients at the wells are obtained as data-read outs at predefined distances along the modelled fracture domain. The set of coupled partial differential equations is implemented and solved with the Finite Element software Comsol Multiphysics v.4.3.

Table 2. Ranges of parameters used for the sensitivity analyses of indicated characteristics of the pressure transients: (a) combined parameter sweep of initial fracture aperture and drained bulk modulus simulating a harmonic flux injection at the pumping well; (b, c) parameter sweep of initial aperture and dry bulk modulus, respectively, for a constant pressure boundary conditions at the pumping well.

Parameter	(a) $p_{\max}$ in pumping well	(b) Reverse response in monitoring wells	(c) Reverse response in monitoring wells
Aperture	$\delta_0 = [0.1 \ldots 5]$ mm	$\delta_0 = [0.2 \ldots 1]$ mm	$\delta_0 = 0.3$ mm
Drained bulk modulus	$K_{\mathrm{d}} = [0.8 \ldots 250]$ GPa	$K_{\mathrm{d}} = 1.4$ GPa	$K_{\mathrm{d}} = [0.7 \ldots 142]$ GPa
Half-length	$a = 1000$ m	$a = 1000$ m	$a = 1000$ m
Boundary condition	harmonic flow ($T = 370$ s)	constant pressure ($\hat{p} = 20$ kPa)	constant pressure ($\hat{p} = 20$ kPa)

2.2.2 *Uncoupled-diffusion approach*

Instead of investigating the fully coupled hydro-mechanical problem, pressure transport along a deformable conduit often has approximatively been addressed by a simple diffusion equation (e.g. Russell & Truitt 1964; van Everdingen & Meyer 1971; Gringarten *et al.* 1974). An uncoupled-diffusion approach relies on the assumption that for some combinations of material parameters or applied boundary conditions the equation governing the fluid flow can be decoupled from the mechanical problem describing the surrounding rock. Hydro-mechanical coupling is accounted for by an effective storage capacity. Here, an uncoupled-diffusion approach is used to investigate which bulk fracture-storage capacity is needed to closely match the basic characteristics of the fully coupled response.

Simple diffusion equations result from the well-known theory of poro-elasticity when the two coupled partial differential equations decouple, for example, the coupling term $\alpha \operatorname{div} \partial \boldsymbol{u}_{\mathrm{s}}/\partial t$ (see poro-elastic equations in Biot 1941) vanishes, where $\boldsymbol{u}_{\mathrm{s}}$ represents the solid displacement of the matrix. Therefore, the poro-elastic equations decouple when the bulk volume of the analysed domain remains constant. When the poro-elastic equations are reformulated in terms of mean stress $\sigma^m = \operatorname{tr}\mathbf{T}/3$ and fluid pressure p, a second condition for decoupling can be formulated, that is, the requirement of constant mean stress σ^m (e.g. Jacob 1940; Detournay & Cheng 1995; Wang 2000). In either case, the poro-elastic equation governing the fluid flow (see Biot 1941) degenerates to a linear diffusion equation

$$\frac{\partial p}{\partial t} - \frac{M\, k^{\mathrm{s}}}{\eta^{\mathrm{f}R}} \operatorname{div}\operatorname{grad} p = 0\,. \tag{3}$$

The difference lies in the exact formulation of the storage modulus M for a material point (see e.g. Wang 2000; Renner & Steeb 2014). When changes in volumetric deformation vanish, that is, $\operatorname{div} \partial \boldsymbol{u}_{\mathrm{s}}/\partial t = 0$, the specific storage capacity

$$s = \frac{1}{M} = \frac{\phi_0}{K^{\mathrm{f}}} + \frac{(\alpha - \phi_0)}{K^{\mathrm{s}}}\,, \tag{4}$$

is related to the fluid bulk modulus K^{f}, to the grain compressibility K^{s}, as well as to the initial porosity ϕ_0, that is, the porosity value around which one linearizes.

Linear diffusion equations have widely been used to model pressure transport along fractures, too. Due to the focus on high-aspect-ratio fractures, one can rely on the radial component of eq. (3) and 'simplistically' replace appearing transport and storage parameters that are initially defined on the level of material points by bulk fracture properties

$$\frac{\partial p}{\partial t} - D_{\mathrm{F}} \frac{\partial^2 p}{\partial r^2} - \frac{D_{\mathrm{F}}}{r} \frac{\partial p}{\partial r} = 0\,. \tag{5}$$

Eq. (5) results also from eq. (1) when assuming that fracture aperture is affected by local pressure variations only and neglecting the convective and the quadratic terms.

The hydraulic diffusivity of the fracture

$$D_{\mathrm{F}} = \frac{\bar{\delta}\, k_{\mathrm{F}}}{S_{\mathrm{F}}\, \eta^{\mathrm{f}R}} \tag{6}$$

is related to fracture permeability k_{F}, to the bulk fracture-storage capacity S_{F}, and to the mean fracture aperture $\bar{\delta} = \langle \delta(r,t) \rangle$ that has to be introduced to account for possible local variations of aperture $\delta(r,t)$ along the fracture. A fracture permeability $k_{\mathrm{F}} = \bar{\delta}^2/12$ results assuming a Poiseuille type of flow in the fracture. In phenomenological analogy to storage capacity's relation to compressibility of fluid and solid in Biot's approach, described in eq. (4), the bulk storage capacity of a planar conduit in a deformable medium is considered to have two contributions (e.g. Dow *et al.* 1982; Ortiz *et al.* 2011; Murdoch & Germanovich 2012; Ortiz *et al.* 2013; Renner & Steeb 2014)

$$S_{\mathrm{F}} = \bar{\delta}\beta_{\mathrm{f}} + \frac{\partial \bar{\delta}}{\partial p}\,, \tag{7}$$

where the first term is related to the fluid compressibility and the second to the contribution from changes in mean fracture aperture $\bar{\delta}$ caused by pressure variations, that is, some measure of fracture stiffness as discussed above. Thus, a single macroscopic value of S_{F} characterizes the storage properties of the fracture in the uncoupled diffusion-approach. In the following, we parameterize storage capacity as

$$S_{\mathrm{F}} = \alpha_{\mathrm{s}}\, \bar{\delta}\, \beta_{\mathrm{f}} \tag{8}$$

for convenience such that the introduced factor α_{s} directly indicates the extent to which storage capacity exceeds the capacity of a rigid fracture, $\bar{\delta}\,\beta_{\mathrm{f}}$. Absolute stiffness values corresponding to a certain α_{s}-value can be calculated according to $\partial\bar{\delta}/\partial p = (\alpha_{\mathrm{s}} - 1)\bar{\delta}\beta_{\mathrm{f}} \approx \alpha_{\mathrm{s}}\bar{\delta}\beta_{\mathrm{f}}$. Physically, the storage multiplier α_{s} quantifies the fluid volume needed in an uncoupled-diffusion model to match the storage capacity of a deformable reservoir. For a physical interpretation of the multiplier α_{s} on the level of an order-of-magnitude estimate, we use the static approximation of the fracture storage capacity as in eq. (2), that is,

$$\alpha_{\mathrm{s},0} = \frac{S_{\mathrm{F},0}}{\bar{\delta}\,\beta_{\mathrm{f}}}\,. \tag{9}$$

Using eqs (6) and (8) in eq. (5) the diffusion equation is thus reformulated as

$$\alpha_{\mathrm{s}}\,\bar{\delta}_0\,\beta_{\mathrm{f}} \frac{\partial p}{\partial t} - \frac{\bar{\delta}_0^3}{12\,\eta^{\mathrm{f}R}} \frac{\partial^2 p}{\partial r^2} - \frac{\bar{\delta}_0^3}{12\,r\,\eta^{\mathrm{f}R}} \frac{\partial p}{\partial r} = 0\,, \tag{10}$$

where the computational complexity is reduced in comparison to the hybrid-dimensional approach (eq. 1), as only the 1-D domain representing the fracture is modelled (Fig. 2). The derivation of eq. (10) relies on a series of assumptions that restrict the applicability of the approach. Eq. (10) is used for homogeneous materials where material parameters do not depend on pressure, that is, changes in fracture aperture due to pressure variations are neglected. Instead, a constant mean aperture $\bar{\delta}_0 = \bar{\delta}(t = t_0)$ is used. Furthermore, convective and non-linear contributions are not accounted for. Also, the parameterization using α_{s} should not defer from the fact that the storage capacity of the fracture is constant, too.

2.2.3 *Analytical solution for periodic radial flow*

As a comparison to numerical models, analytical solutions of the diffusion eq. (10), governing radial fluid flow for a parallel slit, are used for periodic boundary conditions at the injection well. Analytical solutions were presented previously for sinusoidal injection pressure signals and no-flux boundary conditions at $r = a$ (Renner & Messar 2006). When transformed to the frequency domain, the periodic pressure transients at the pumping borehole as well as at the monitoring boreholes are characterized by a phase φ_i for the imposed period T and an amplitude A_i. Phase differences $\Delta\varphi_i = \varphi_i - \varphi_0$ and amplitude ratios $R_i = A_i/A_0$ between signals at monitoring wells (index i) and the pumping well (index 0) are interpreted to give insight into the flow along the fracture.

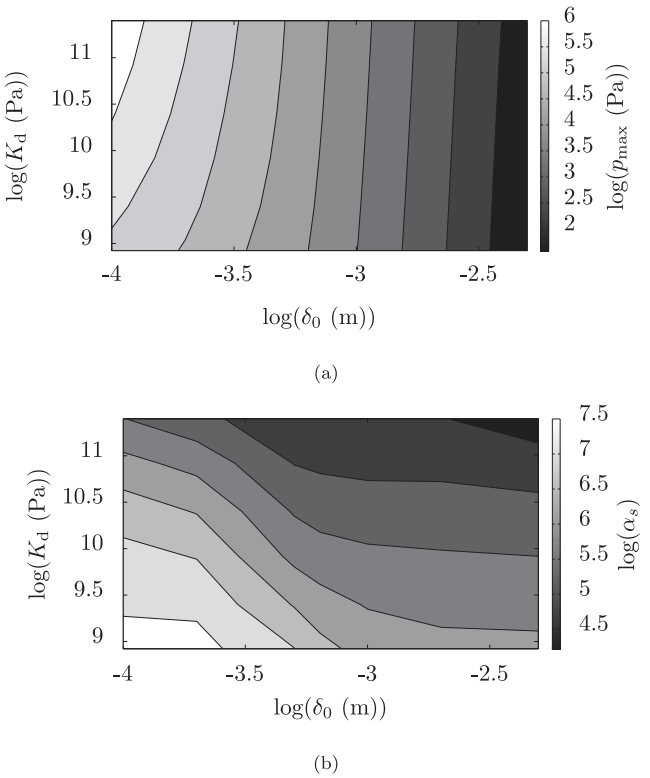

Figure 3. (a) Contour of logarithm of pressure p_{max} at monitoring borehole and (b) contour of logarithm of storage multiplier α_s for combinations of initial aperture δ_0 and dry modulus K_d from 0.1 to 5 mm and 0.8 to 250 GPa, respectively. The parameter sweep was actually performed for the Young's modulus E, keeping the Poisson's ratio constant at $\nu = 0.3$, which resulted in a sweep in $K_d = E/2(1-2\nu)$ and $G = E/2(1+\nu)$ with a constant ratio of $K_d/G = 3.25$.

Analytical solutions of the uncoupled-diffusion approach provide characteristic lines in the phase-shift amplitude-ratio domain to which numerical results can be conveniently compared. The analytical solution weakly depends on the monitoring distance; with increasing distance, the characteristic line in the phase-shift amplitude-ratio domain shifts downwards (see fig. 4 in Renner & Messar 2006). In this investigation, the analytical solution for $r = 5$ m is used, that is, 100 times the well radius r_w. The 'master curves' for a specific monitoring distance do not, however, depend on α_s since the solutions are self-similar in r^2/DT (e.g. Weir 1999).

2.3 Processing and analysis of numerical data

The use of periodic signals allows us to employ FFT analysis to determine the phase shifts $\Delta\varphi_i$ and the amplitude ratios R_i of the pressure transients $p_i(t)$ at the monitoring boreholes with respect to the pressure $p_0(t)$ at the injection well. Analysis in the frequency domain provides the phase shift between two signals within a common period. Signals were checked by eye for cases when the phase shifts $\Delta\varphi_i$ exceeded one period. Transient non-oscillatory phases within the first pumping cycles were deleted from the pressure records before their transformation to the frequency domain. In some cases a tapered cosine window was used to ensure that the section of the pressure transient considered for transformation started and ended with identical values.

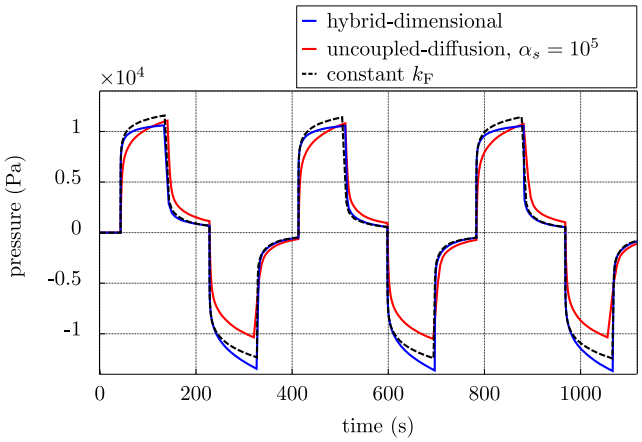

Figure 4. Transient pressures at the pumping well for a pumping period $T = 370$ s, initial aperture $\delta_0 = 640$ μm and fracture half length $a = 1000$ m. Solutions of the hybrid-dimensional approach with full hydro-mechanics (blue line), with the uncoupled-diffusion approach ($\alpha_s = 10^5$, red line), and with the hybrid-dimensional approach and a constant fracture permeability $k_F = \bar{\delta}_0^2/12$ in eq. (6) (dashed black line). Matching between the hydro-mechanically coupled results and the uncoupled results was performed based on the amplitude of pressure oscillations during the injection phases.

3 RESULTS

We produced synthetic data for periodic pumping tests employing (1) the hybrid-dimensional (eq. 1) and (2) the uncoupled-diffusion (eq. 10) approach. The hybrid-dimensional approach is considered to yield the full behavior and the diffusion equation to be intrinsically correct only for undeformable rocks. Pressure transients are qualitatively compared in the time domain but an extensive quantitative comparison is restricted to the frequency domain. First, the pressure transients are separately analysed in the pumping and monitoring wells, and the sensitivity of the maximum pressure reached in the monitoring borehole, p_{max}, to geometrical and material properties (Table 2a) is investigated. The sensitivity of the storage multiplier α_s, needed to fit simple-diffusion results to the fully coupled ones, is analysed with respect to variations in input parameters. Finally, an interference analysis is performed comparing pressure values at the injection and monitoring wells.

3.1 Pressure analysis in the time domain

3.1.1 Pumping well

Depending on the combination of δ_0 and K_d, pressure values at the pumping well reach $p_{max} \sim$ ˜0.1 kPa (for large apertures and compressible rocks, that is, low drained bulk modulus K_d) or $p_{max} \sim$ 1 MPa (for thin fractures and rigid rocks), Fig. 3(a). On the one hand, pressure is strongly sensitive to fracture aperture. Changes of δ_0 affect fracture permeability as well as the relative importance of hydro-mechanical coupling phenomena to diffusion processes. On the other hand, pressure values are weakly sensitive to K_d for large apertures, but for $\delta_0 < 1$ mm, where values of p_{max} more strongly depend on the values of the dry bulk modulus K_d with decreasing initial aperture δ_0.

The fully coupled approach yields a peculiar asymmetry in the pressure transient at the injection well (Fig. 4). Pressure excursions from the initial pressure remain smaller during injection than during production. A similar asymmetry in the pressure transient has also been observed during field experiments, (e.g. Renner &

Messar 2006; Schweisinger *et al.* 2009). Also pressure transients during pumping phases and during subsequent shut-in phases are not simply inverted for the hybrid approach while they are for the uncoupled-diffusion approach as expected for insignificant leak-off. During shut-in phases pressure varies less rapidly than during the preceding injection and the succeeding production phases. Asymmetry in the pressure profile is reduced neglecting variations of the fracture permeability due to solid deformations in the hydro-mechanical coupled model. The uncoupled-diffusion approach can approximate the transient obtained with the fully coupled hydro-mechanical model when α_s is chosen appropriately, but the asymmetry of the pressure profile between injection and production phases is less pronounced and is only an apparent result related to the brevity of the non-pumping-period during which the initial pressure level is not reached, that is, asymmetry switches with a switch in the starting pumping operation.

For the chosen combinations of apertures and rock bulk moduli (Table 2a), the storage multiplier that leads to the best match between the pressure transients in the pumping well obtained with the hybrid-dimensional approach and the uncoupled-diffusion approach varies by over three orders of magnitude, from $\alpha_s \sim 10^{4.5}$ to $\alpha_s \sim 10^{7.5}$ (Fig. 3b). The storage multiplier strongly depends on the drained bulk modulus of the rock, independent of the chosen initial aperture δ_0. In a weaker way it also depends on fracture aperture. Matching of the pressure profiles was performed with respect to the pressure amplitude during injection phases only, as neither the asymmetry nor the curvature of pressure profiles obtained with the hybrid-dimensional approach could be reproduced using the uncoupled-diffusion approach (Fig. 4).

3.1.2 Monitoring wells

The fully coupled approach yields pressure transients that are more and more dominated by oscillations related to reverse responses for increasing monitoring distance where in general amplitudes have largely decreased in comparison to the pumping well. At $r = 15\,\text{m} = 0.015\,a$, the reverse response is a short pressure perturbation with opposite direction compared to the pumping well, taking place shortly after a change in injection boundary condition, and superposed on pressure oscillations driven by diffusion. At $r = 50$ m, contributions from hydro-mechanical coupling evidenced by the reverse response are larger than pressure oscillations caused by diffusion. At distances $r > 90$ m, pressure variations are uniquely caused by reverse-pressure response and oscillations caused by pressure diffusion alone can be neglected (Fig. 5).

Numerical results of the uncoupled-diffusion approach approximate the fully coupled solutions at the pumping well only (Fig. 4) and amplitude reduction with increasing monitoring distance is more pronounced than in the solutions of the hybrid-dimensional approach (Fig. 5), as the penetration depth of the diffusive pressure front is limited. Furthermore, the uncoupled-diffusion approach fails to capture hydro-mechanical coupling effects that take place along the fracture, e.g. the reverse response (Slack *et al.* 2013; Vinci *et al.* 2014a).

3.1.3 Sensitivity of reverse response to fracture aperture and rock dry modulus K_d

Reverse-pressure response is a prominent evidence of the importance of hydro-mechanical effects during pumping operations. To facilitate direct comparison of the pressure transients along the fracture resulting from the range of parameters employed (Fig. 6), a pressure boundary condition $\hat{p} = 20$ kPa is applied at the pumping well, instead of a flux boundary condition, that corresponds more closely to field experiments.

The magnitude of the reverse-response effect diminishes with increasing aperture and constant fracture length (see Table 2b for parameters used), actually vanishing for very wide fractures (Fig. 6, left). For the latter case, the hydro-mechanical coupling becomes negligible because the relative magnitude of the fracture deformation decreases with increasing aperture. The additional storage caused by fracture deformation becomes negligible for wide fractures and pressure-transport processes are faster compared to conduits with smaller aperture. The reverse response to pumping quantitatively decreases for increasing values of K_d of the surrounding rock (see Table 2b and c for parameters used). For $K_d = 0.7$ GPa, pressure values drop to $p = -4$ kPa (20 per cent of $\hat{p}$) before diffusion effects take place, while no reverse response occurs for an ideally rigid fracture. The sensitivity of the magnitude of the reverse response to the initial fracture aperture and to the drained modulus of the surrounding rock qualitatively agrees with the results obtained by Slack *et al.* (2013) using slug tests. Apparently, the initial fracture aperture associated with the maximum reverse response is not constant but depends on the choice of the fracture stiffness (in our investigations on K_d).

The duration of the reverse response is qualitatively analysed as the time from the beginning of injection until pressure at monitoring points reaches again the initial value p_0. The time extent of reverse responses varies with the position along the fracture and is related to the drained bulk modulus of the rock in a non-unique way. Given the used input parameters (Table 2c), the duration of reverse response has a maximum around $K_d \sim 1.4$ GPa. For $K_d < 1.4$ GPa, the duration of reverse response is proportional to the drained modulus of the rock. For $K_d > 1.4$ GPa, the reverse response vanishes more rapidly with increasing drained bulk modulus (Fig. 6, right).

The duration of reverse response affects the pressure propagation along the fracture. Time t_{eq} needed to reach the prescribed pressure $\hat{p}$ at the injection well throughout the entire fracture length depends on K_d. On the one hand, for $K_d > 14$ GPa, t_{eq} is proportional to the drained modulus. Along rigid fractures a steady-state solution is reached faster than for deformable fractures. Hydro-mechanical coupling effects, which slow down the diffusion process, diminish for large values of K_d. On the other hand, t_{eq} is inversely proportional to the drained modulus for $K_d < 1.4$ GPa. Along weak fractures, pressure transport is facilitated by large deformations, which increase the fracture transmissivity. Time t_{eq} reaches a maximum for $1.4\text{GPa} < K_d < 14$ GPa, where pressure transport is slowest (Fig. 6, right).

3.2 Pressure analysis in the frequency domain

Phase shifts between the pressure signals at the pumping borehole and the monitoring wells increase with increasing monitoring distance r up to 90 m, that is, 9 per cent of the fracture length, while amplitude ratios R_i decrease. The fully coupled calculations yield $\Delta\varphi_i = 0.052$ to 1.1 cycles and $R_i = 0.25$ to 7×10^{-4}. The uncoupled-diffusion approach yields $\Delta\varphi_i = 0.11$ to 1.56 cycles and $R_i = 0.18$ to 4.5×10^{-6} (Fig. 7a). For larger distances, that is, 90 m $\leq r \leq$ 550 m, only the fully coupled approach gives

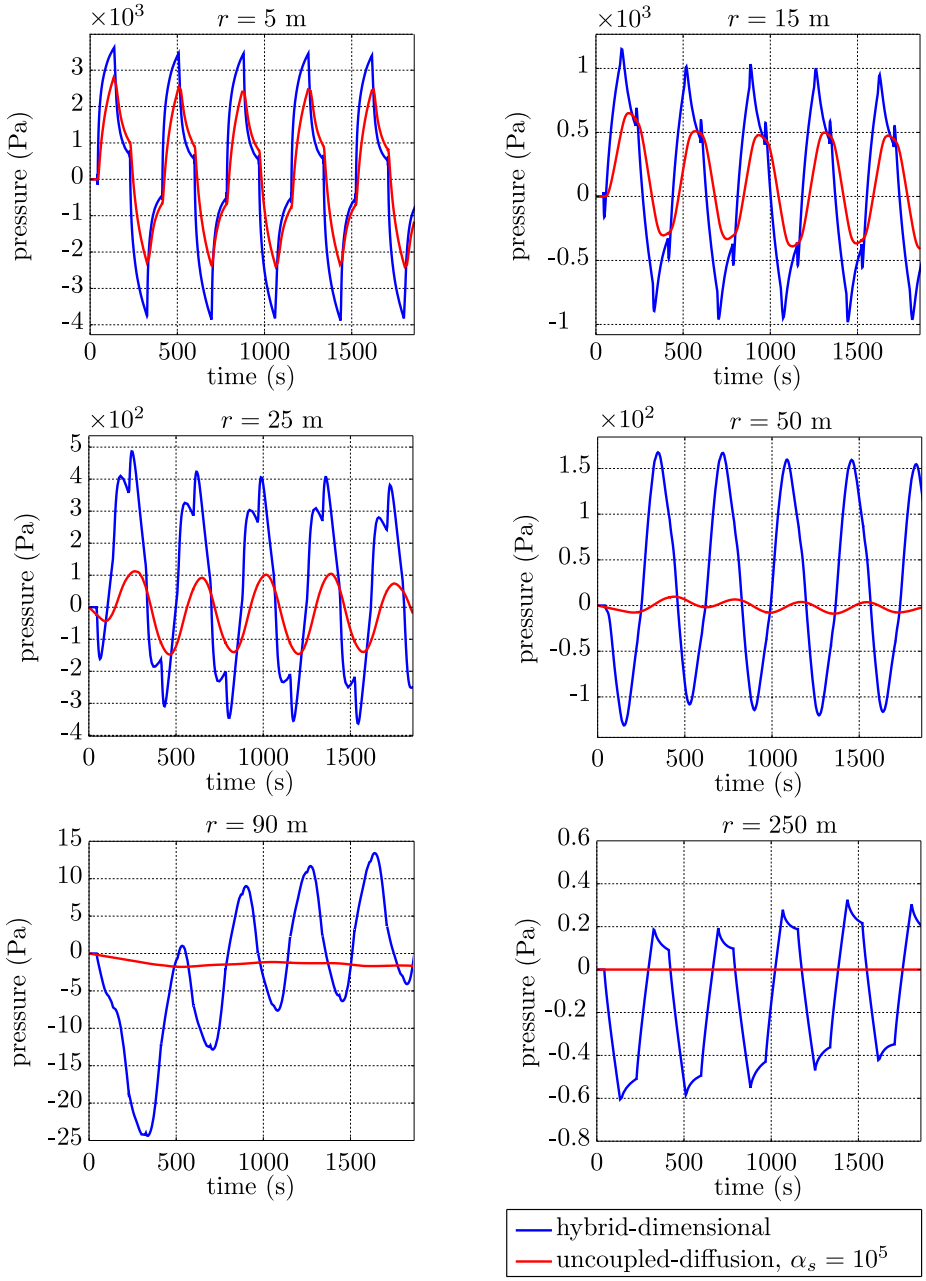

Figure 5. Transient pressures at monitoring boreholes at $r = 5$, 15, 25, 50, 90, and 250 m for a pumping period $T = 370$ s, initial aperture $\delta_0 = 640$ μm and fracture half length $a = 1000$ m. Solutions of the hybrid-dimensional approach with full hydro-mechanics (blue line) and with the uncoupled-diffusion approach ($\alpha_s = 10^5$) (red line).

significant pressure perturbations (associated with reverse response). At $r = 550$ m, phase shift and amplitude ratio are 0.7 and 5.1×10^{-6}, respectively.

Despite corresponding to largely different values of α_s, numerical solutions ($\alpha_s = 10^5$) obtained using the uncoupled-diffusion approach fall on the master curve of the analytical solution, in accord with the self-similarity predicted from the analytical solution. Results for different periods plot at different sections of the master curve, also in accord with self-similarity. The modest mismatch with increasing phase shift is readily explained by the weak dependence of the analytical solution on the actual distance of the monitoring wells. Here, we present the analytical solution for $r = 5$ m (Fig. 7a) but for larger monitoring distances the curve representing the analytical shifts downwards. Numerical results of the fully coupled solution closely follow the analytical solution only for small phase shifts $\Delta\varphi_i$ and amplitude ratios (Fig. 7a). With increasing amplitude reduction, results of the hybrid-dimensional approach deviate from the analytical solution and exhibit larger phase shifts and larger amplitude ratios in comparison to the uncoupled-diffusion approach. For $\log(R_i) < -3$, phase shift values converge to $\Delta\varphi_i \sim 0.7$ whereas amplitude ratios keep decreasing.

Three domains can be identified from the differences between the results for the uncoupled-diffusion approach and the hydro-mechanical approach. These fields can be visualized along the spatial domain of the fracture (Fig. 7b) when monitoring positions are

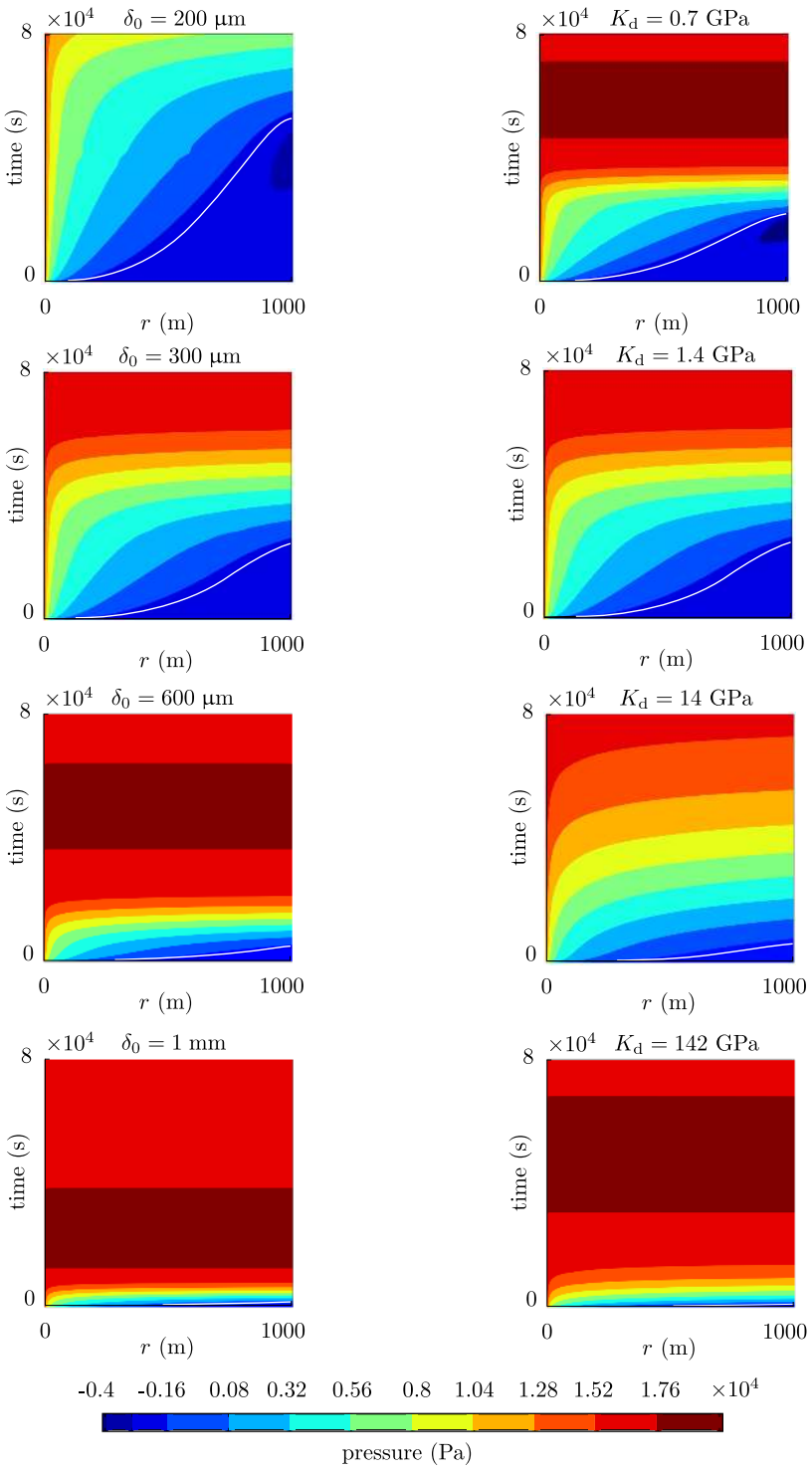

Figure 6. Contours of pressure p in the fracture (horizontal axis) for the time domain $t = 0$ to 8×10^4 s (vertical axis). Pressure transport is induced by the pressure boundary condition $p(r_w) = \hat{p}$ at the injection well: (left) for $\delta_0 = 0.2$–1 mm and $K_d = 1.4$ GPa; (right) for $\delta_0 = 0.3$ mm and $K_d = 0.7$–142 GPa. The shear modulus was covaried with the bulk modulus of the dry rock to maintain a constant ratio of 3.25 (see caption of Fig. 3). The white lines enclose the reverse response ($p = p_0$). For configurations where pressure transport is fast, pressure ultimately decreases in the considered time span due to leak-off effects.

normalized by the diffusion length of an undeformable fracture, $L_{diff} = \sqrt{D\,T}$, with $D = \delta_0^2/(12\,\eta^{f R}\beta_f)$, that is, $r^\star = r/L_{diff}$. In the vicinity of the pumping well ($r^\star \sim 0$ to 0.0025), phase shift is related to diffusive pressure propagation only. Phase shift values of either numerical approach and the analytical solution are comparable. Further away ($r^\star \sim 0.0025$ to 0.01), hydro-mechanical coupling effects become larger and affect the phase shift values. In this domain of the fracture, measured phase shifts are the result of the sum of both diffusion and hydro-mechanical processes. In the vicinity of $r^\star \sim 0.009$ (at $r \sim 90$ m), as diffusion effects vanish, pressure

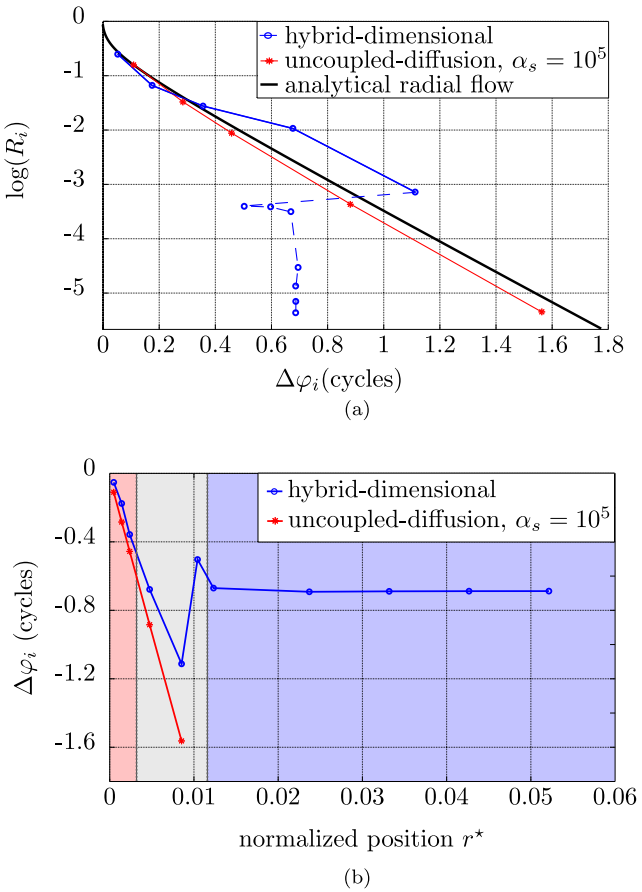

Figure 7. Results of a numerical pumping test with period $T = 370$ s, $\delta_0 = 0.64$ mm and $a = 1000$. From left to right the markers related to the full line identify $r = 5$, 15, 25, 50, 90; (a) logarithm of amplitude ratios R_i versus phase shifts $\Delta\varphi_i$ of the transient pressure in the monitoring boreholes with respect to the pressure in the pumping well. Amplitudes and phase shifts are larger in the hydro-mechanical model, as a result of reverse response. The jump in phase shift and convergence to $\Delta\varphi_i \sim 0.7$ are also caused by hydro-mechanical coupling. The markers related to the blue dotted line represent phase shift values at $r = 110$–550 m; (b) phase shift against distance $r^\star$, normalized with respect to the diffusion length. In the vicinity of the injection well diffusion dominates (red domain). For intermediate distances diffusion and reverse response coexist (gray domain). At the largest distances, transient pressure is a response to hydro-mechanical coupling only (blue domain).

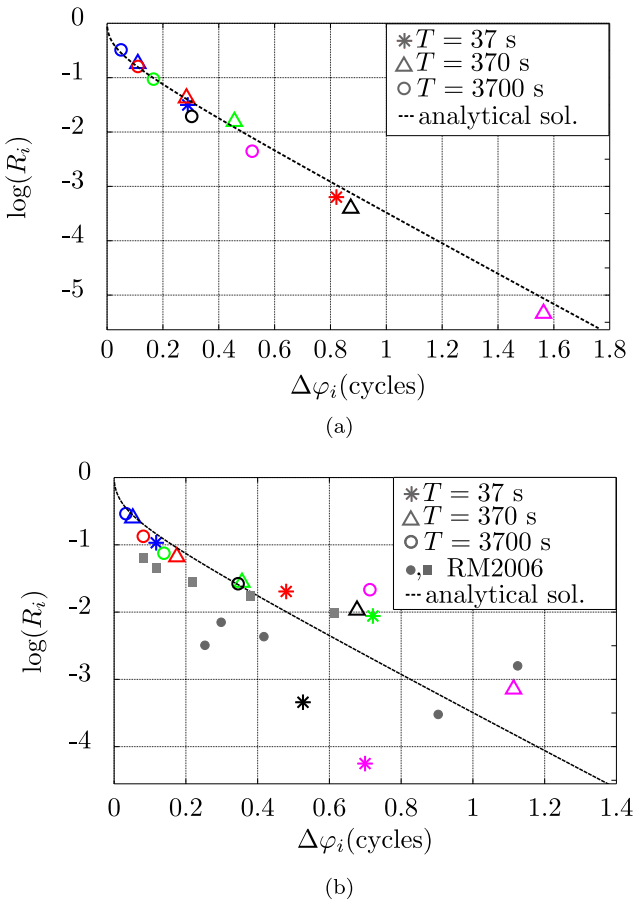

Figure 8. Logarithm of amplitude ratios R_i versus phase shifts $\Delta\varphi_i$ at monitoring boreholes at positions $r = 5$ m (blue), $r = 15$ m (red), $r = 25$ m (green), $r = 50$ m (black) and $r = 90$ m (magenta) for different pumping periods ($T = 37$, 370 and 3700 s), obtained with (a) the uncoupled-diffusion approach and (b) the hybrid-dimensional approach. Experimental data obtained by Renner & Messar (2006) (RM2006) for selected tests ($T = 60$, 180, 600, 1800 and 5400 s) at two monitoring points (gray) fall persistently under the master curve for small phase shifts but also above for large phase shifts.

variations in the first period of pumping become visible. From a distance $r^\star \sim 0.009$ the phase shift values decrease to $\Delta\varphi_i < 1$ (Fig. 7b). With increasing distance from the pumping well ($r^\star \geq 0.01$) phase shift values are related to the hydro-mechanical response only.

The qualitative distribution of phase shift values in the three domains along the fracture (Fig. 7b) is valid in general but quantitatively the normalized distances separating the three domains depend on the pumping period T. The relative sizes of the three domains vary depending on the diffusion characteristics as well as on the hydro-mechanical coupling effects. Different pumping periods trigger different pressure profiles along the fracture. For $T = 37$ s, pressure penetration depth due to diffusion along the fracture is smaller than for $T = 370$ or $T = 3700$ s. The region dominated by diffusion is also small. Therefore, the domain characterized by reverse response begins closer to the pumping well in comparison to large period injections (Fig. 8b). For small pumping periods, amplitude reduction is large and phase shifts at the monitoring wells converge near to the injection point. For $T = 37$ s, the phase shift induced by reverse response occurs at $r = 90$ m and is $\Delta\varphi_i \sim 0.7$. Phase shift induced by reverse response only is quantitatively equal to the one obtained for a pumping period $T = 370$ s (Fig. 7), with the difference that for $T = 370$ s convergence of $\Delta\varphi_i$ occurs at $r = 120$ m.

4 DISCUSSION

In the following discussion, we first focus on the pressure distribution in the fracture as affected by hydro-mechanical coupling. The pressure distribution is of paramount importance for understanding operations like hydraulic stimulations. The severe limitations associated with the point-wise information from the pumping well (and in cases monitoring wells) can be alleviated by varying the pumping protocol and substantial modelling of recorded transients. Pumping protocol strongly affects to which extent hydraulic and mechanical processes are activated. A central task is to develop pumping protocols that best constrain the model to be employed. Reverse response to pumping, for example, occurs only when flow rate at the injection well is changed rather abruptly. Application

of non-harmonic signals at the injection well replicates reverse response various times for each cycle. Periodicity of signals allows for usage of fast Fourier transformation and thus for frequency-domain analysis of responses too small to be discerned in the time domain. The diagnostic potential of transfer functions in the amplitude-ratio phase-shift domain are highlighted using our parametric sweeps for different models in comparison to simple diffusion analysis.

4.1 The role of hydro-mechanical effects for the pressure distribution in the fracture

4.1.1 Pressure asymmetry at the pumping well

The simulations using the hybrid-dimensional approach yield asymmetric pressure records in particular at the pumping well (Fig. 4) in close resemblance to records of field experiments (Renner & Messar 2006; Schweisinger *et al.* 2009). Besides mismatch between pumping and shut-in phases, pressure excursions are smaller during injection than during production. Asymmetry in pressure profiles does not seem to be related to the specifics of the fracture geometry, but rather linked to the presence of hydro-mechanical coupling effects. Fractures appear to respond mechanically in different ways during injection and production due to the non-local property of deformation. The asymmetry of the pressure profile is mostly related to variations in fracture permeability associated with aperture-altering deformations as shown by the significant reduction in anisotropy resulting from fixing the fracture permeability as a constant property (Fig. 4). During injection, the fracture permeability increases due to fracture widening, while during production the permeability decreases due to fracture narrowing. The largest permeability variations occur close to the pumping well, where the greatest deformations take place. Thus, the fracture-entry permeability seems crucial for the hydraulic behaviour of the fracture. Possibly, some effects related to permeability variations in the vicinity of the wellbore, referred to as wellbore or fracture skin effects (e.g. Moench 1984), might to some extent be related to hydro-mechanical effects.

4.1.2 Reverse response to pumping

At large distances from the injection well, pressure oscillations are induced by fracture deformation only. Intuitively, the reverse response is expected to correspond to a phase shift $\Delta\varphi_i = 0.5$, that is, opposite to the phase of the pressure at the injection well. Yet, such a phase shift of 0.5 holds only in the limit case of an incompressible fluid for which pressure diffusion is instantaneous. For a compressible fluid, local deformation and consequently local pressure changes are the result of pressure variations occurring not only at the pumping well, but also at all points along the fracture. The phase shift $\Delta\varphi_i \sim 0.7$ of pressure oscillations caused exclusively by the reverse response is a convolution of phase shifts of pressure values acting at all points in the fracture, weighted by pressure amplitude and distance. Further analyses are necessary to constrain in detail the relation of the limit assumed by the hydro-mechanically induced phase shift and the geometrical characteristics of the fracture as well as the material parameters of the solid rock and of the fluid.

4.1.3 Influence of pumping period on hydro-mechanical signature

Diagnostic pattern regimes of phase-shift and amplitude-ratio values were identified (Fig. 7b) that however depend on the chosen pressure-penetration depth along the fracture and, therefore, on the pumping period T (Fig. 8b). For a fracture with given geometrical and material properties, a larger or smaller pumping period results in a larger or smaller domain along the conduit, dominated by diffusion. Deviation from the analytical solution and convergence to a limiting phase-shift value controlled by the reverse response occur at different positions along the fracture depending on T (Fig. 8b). Whereas the position in the fracture where diffusion vanishes depends on the pumping period, the value to which phase shifts converge seems to be insensitive to T. For both, $T = 37$ s and $T = 370$ s, $\Delta\varphi_i$ converges to $\sim$0.7 (Figs 7a and 8b). For $T = 3700$ s, pressure-penetration depth caused by diffusion is larger than the monitored distances and the region dominated by the reverse response was not captured by the numerical results.

4.2 Diagnostic potential of periodic tests for hydro-mechanical signature

Periodic pumping tests provide a robust diagnostic tool for hydro-mechanical effects beyond singular reverse responses during constant-rate pumping that could easily be hidden in noisy pressure records. The periodic characteristic of the applied injection boundary condition permits using FFT techniques to analyse data even slightly below the digital resolution (Renner & Messar 2006). A single periodic pumping test yields values for the phase shift and the amplitude ratio that—in comparison to the solution of the uncoupled-diffusion approach—may already allow for significant interpretation regarding the validity of the diffusion approach but also for the contribution of hydro-mechanical coupling. Data obtained with the hybrid-dimensional approach persistently fall under and over the master curve related to radial flow for low-frequency (small $\Delta\varphi$) and high-frequency (large $\Delta\varphi$) pumping tests, respectively. Renner & Messar (2006) also observed this characteristic behaviour in their field tests (Fig. 8b).

The hydro-mechanical signature in pressure profiles along the fracture prominently comprises the asymmetric pressure transient at the pumping well (Fig. 4) as well as the reverse-pressure response observed at various monitoring points (Fig. 5). Simulated pressure transients differ qualitatively and quantitatively during pumping and shut-in, but also between injection and production phases. Further investigations are needed to analyse the relative relevance of additional causes for asymmetrical pressure transients, for example leak-off. On the one hand, asymmetry related to hydro-mechanical effects depends on the direction of fracture deformation, that is, whether the fracture is opening or closing, and therefore on the related permeability variations. On the other hand, leak-off effects, that is, loss/gain of fluid mass into/from the surrounding rock matrix, depend on the value of the pressure in the fracture, relative to the initial pressure. Future investigations should consider both contributions, the direction of fracture deformation and the pressure level in the fracture, to asymmetrical pressure transients and their interaction for different pumping operations, that is, shut-in and production phases.

4.2.1 The storage multiplier α_s as a characterizing (physical) parameter

The storage multiplier α_s in eq. (10) quantitatively describes the fracture normal stiffness, which is closely related to pressure-induced aperture changes contributing to fracture storage capacity. We focus on the storage of the fracture because it is the property

that is most affected by the hydro-mechanical effects and, at the end, when investigating reservoirs, storage capacity is of major interest, as it quantifies the yield. Our choice of model parameters (Table 1) was guided by the previously presented modelling of field observations (Vinci *et al.* 2014a). At face value, corresponding stiffness values ranging from 10^{-3} to 10^{-1} MPa/mm fall in the lowest range of fracture-stiffness data from laboratory experiments (Bandis *et al.* 1983; Barton *et al.* 1985). This order in values may reflect that field data from shallow boreholes were used for constraining parameters and that a fracture with an enormous length in comparison to lab-scale experiments is considered. We also vary stiffness by more than two orders of magnitude by considering quite large bulk moduli.

While the ranges of numerical values and analytical estimates for the storage multiplier appear similar, the correspondence between the obtained storage multiplier and the static approximation is actually not that close for an individual calculation. For example, in the main set of calculations the storage multiplier $\alpha_s = 10^5$ was used (with $\delta_0 = 640$ μm, $T = 370$ s), which yields an optimal approximation of the transients at the *pumping well*. For these calculations, the value of the storage multiplier deviates by a bit more than one order of magnitude from the one obtained with the static approximation following eqs (2) and (9) ($\alpha_s = 1.8 \times 10^6$). Thus, matching hydro-mechanical response at the pumping well by diffusion calculations requires a somewhat lower storage capacity than expected from the simple approximation of the bulk storage capacity after Valkó & Economides (1995), opposite to what is found for the response of *monitoring wells* (see Renner & Steeb 2014). In the current study, matching of p_{max} values was performed at the pumping well only. Approximation of the pressure transients along the fracture domain would require different values of α_s at each monitoring point.

4.2.2 Limitations of the uncoupled-diffusion approach

The numerical ease of the diffusion approach is tempting. Yet, reducing the fracture-storage capacity to a single value representing the entire domain is a limiting assumption. Employing the uncoupled-diffusion approach and a single macroscopic value for the storage capacity, only the pressure transient at the injection well can be fitted (Fig. 4). Hydro-mechanical effects caused by spatial and temporal changes of the fracture-storage capacity, for example, reverse-pressure response, are neglected and pressure transients at monitoring boreholes cannot be consistently matched. With this observation in mind, particular caution is needed by practitioners when an uncoupled-diffusion approach is used to model the pressure records from a single well (see also Murdoch & Germanovich 2012). Numerical results from an uncoupled-diffusion approach that match the signal at the pumping well fairly well may lead to erroneous predictions regarding the pressure distribution at some distance from the injection well. The scaling relation used to analyse, for example, induced seismicity (e.g. Shapiro *et al.* 2005; Shapiro & Dinske 2009) may therefore have to be reconsidered.

Within the uncoupled-diffusion approach the storage multiplier is a quantitative index of the storage capacity of the fracture related to its deformation (Fig. 3b). For $\alpha_s = 1$, storage is solely due to fluid compressibility. The more compressible the matrix and/or the thinner the fracture the higher the values of α_s (eqs 2 and 9). The fracture-storage capacity may exceed storage deriving from fluid compressibility alone by several orders of magnitude. Even for a relatively wide fracture, for example, $\delta_0 = 5$ mm, in a rock with an unrealistically high drained modulus, for example, $K_d = 250$ GPa, a storage multiplier of $\alpha_s \sim 10^4$ is required to match the pressure transient from the hydro-mechanically coupled calculation at the pumping well (Fig. 3b). This value exceeds the static approximation, using eqs (2) and (9), of 2.5×10^3 but agrees within order of magnitude. Thus, evaluating *in situ* data with the uncoupled-diffusion approach will not lead to a suspicious estimate of storage properties per-se. Yet, if records in monitoring wells were also available, then matching pressure transients would require a different value of α_s at each monitoring position. Traditionally, then a heterogeneous rock formation would be invoked to explain variations in the values of α_s with increasing distance from the pumping well. Such conventional interpretation should be reconsidered in the light of the presented numerical results of the hybrid dimensional approach. The mismatch between the matching storage parameter of $\alpha_s \sim 10^4$ (Fig. 3b) and the stationary estimate may indicate that effects other than diffusion of a compressible fluid cannot be neglected. While specific investigation of wide fractures was not the scope of this work, dimensional analyses showed that phenomena such as convection and nonlinear/quadratic effects complement diffusion and hydro-mechanical coupling for configurations involving rigid and/or wide fractures and fluids other than water (Vinci *et al.* 2014a).

5 CONCLUSIONS

Understanding the role of hydro-mechanics is essential for the interpretation of pressure transients during well testing. Periodic pumping tests were simulated considering a vertical injection well intersecting a single horizontal deformable fracture. Pressure transients along the fracture were monitored at the injection point as well as at some distance from it. Modelling was performed using two methods, a hybrid-dimensional hydro-mechanical approach and an uncoupled-diffusion approach. The results of the coupled and the non-coupled models were compared to analytical solutions of the uncoupled problem. The uncoupled-diffusion approach, which is based on a simplified storage capacity concept, fails to capture the hydro-mechanical response of the fracture and fits the hydro-mechanical results only at a single point at a time. Some results were analysed in the time domain, but extensive comparison and post processing were performed in the frequency domain using fast Fourier transformation, showing the great diagnostic potential of periodic pumping tests. Phase shifts and amplitude ratios between pressure signals at the monitoring and injection points exhibit characteristics deviations from the expected uncoupled-diffusion results due to the contribution of reverse-pressure response, an exclusive phenomenon of coupling. With increasing monitoring distance or decreasing pumping period, phase shifts and amplitude ratios deviate from diffusion-based analytical solutions and phase shifts converge to a constant value. Unlike for simple diffusion, the results of the coupled problem in the amplitude-ratio phase-shift domain depend on the pumping period that affects the diffusive pressure penetration depth as well as the extent of fracture deformation along the fracture domain.

Pressure transients in a deformable conduit strongly depend on the initial fracture aperture and, for small apertures, are also greatly affected by the drained modulus of the surrounding material. Hydro-mechanical effects are more important for deformable host rocks and for conduits with high aspect ratios. Fracture permeability is particularly affected by the pressure distribution. Pressure-related evolution of permeability in the vicinity of the pumping well leads to contrasting pressure records during pumping and shut-in phases

as well as injection and production phases. This asymmetry bears implications for the provision of deep geothermal energy that inevitably requires production of hot water and re-injection of cold water. Furthermore, the pressure distribution in a deformable fracture does not simply comply with the standard scaling relation of uncoupled diffusion possibly requiring reconsideration of the common interpretation strategies for induced seismicity. Finally, periodic testing promises improved resolution of fracture (or more general reservoir) deformation from the installation of tiltmeter or strainmeter at the surface thanks to the benefits of massive filtering for the excited periods.

NOTATION

a [m]	fracture half-length
A_i [Pa]	pressure amplitude at monitoring wells
A_0 [Pa]	pressure amplitude at injection well
D_F [m s^{-1}]	fracture diffusivity
D [m^2 s^{-1}]	diffusion coefficient
G [Pa]	shear modulus of the dry rock
K_d [Pa]	bulk modulus of the dry rock
K^f [Pa]	bulk modulus of the fluid
K^s [Pa]	grain bulk modulus of the solid
k_F [m^2]	fracture permeability
k^s [m^2]	intrinsic permeability
L_diff [m]	diffusion length
L_i [m]	distance between injection and monitoring boreholes
M [Pa]	storage modulus
p [Pa]	fluid pressure measured relative to p_0
$\hat{p}$ [Pa]	pressure boundary condition
$\bar{p}$ [Pa]	average pressure along the fracture
p_0 [Pa]	initial pressure
p_eq [Pa]	pressure at steady state
p_max [Pa]	maximum pressure reached at injection well
p_matrix [Pa]	pressure in the rock matrix
q [m^3 s^{-1}]	fluid flux
$\hat{q}$ [m^3 s^{-1}]	flux boundary condition
q_L [Pa s^{-1}]	source term related to leak-off
r [m]	radial component of the position vector
r_w [m]	radius of boreholes
$r^\star$ [-]	normalized position
R_i [-]	amplitude ratios at monitoring points
S_F [mPa^{-1}]	fracture-storage capacity
$S_{\mathrm{F},0}$ [mPa^{-1}]	static approximation of the fracture-storage capacity
s [Pa^{-1}]	specific storage capacity
t [s]	time
t_eq [s]	time to reach a steady state
T [s]	pumping period
$\mathbf{T}$ [Pa]	total stress
$\mathbf{u}_\mathrm{s}$ [m]	displacement of the solid phase
α [-]	Biot-Willis parameter
α_s [-]	storage multiplier
$\alpha_{\mathrm{s},0}$ [-]	static approximation of the storage multiplier
β_f [Pa^{-1}]	isothermal fluid compressibility
δ [m]	fracture aperture
$\bar{\delta}$ [m]	mean fracture aperture
δ_0 [m]	initial fracture aperture at the pumping well
$\bar{\delta}_0$ [m]	initial mean fracture aperture
$\Delta\varphi_i$ [-]	phase shifts at monitoring points
$\eta^{\mathrm{f}R}$ [Pa s]	effective viscosity of the fluid
ν [-]	Poisson's ratio
σ^m [Pa]	mean stress
ϕ_0 [-]	initial porosity
φ_i [-]	signal phase at monitoring wells
φ_0 [-]	signal phase at injection well

ACKNOWLEDGEMENTS

We would like to gratefully acknowledge the financial support of the collaborative research center SFB 526. The insightful reviews of two anonymous reviewers are greatly appreciated.

REFERENCES

Bandis, S., Lumsden, A. & Barton, N., 1983. Fundamentals of rock joint deformation, *Int. J. Rock Mech. Min. Sci. Geomech. Abstr.,* **20,** 249–268.

Barton, N., Bandis, S. & Bakhtar, K., 1985. Strength, deformation and conductivity coupling of rock joints, *Int. J. Rock Mech. Min. Sci. Geomech. Abstr.,* **22,** 121–140.

Becker, M. & Guiltinan, E., 2010. Cross-hole periodic hydraulic testing of inter-well connectivity, in *Stanford Geothermal Workshop, SGP-TR-188,* Stanford University, Stanford, CA, USA.

Berg, S., Illman, W. & Mok, C., 2014. Joint estimation of hydraulic and poroelastic parameters from a pumping test, *Groundwater,* doi:10.1111/gwat.12271.

Biot, M.A., 1941. General theory of three-dimensional consolidation, *J. Appl. Phys.,* **12,** 155–164.

Black, J. & Kipp, J.K., 1981. Determination of hydrogeological parameters using sinusoidal pressure tests: a theoretical appraisal, *Water Resour. Res.,* **17,** 686–692.

Bruggeman, G., 1999. *Analytical Solutions of Geohydrological Problems,* Elsevier.

Cappa, F., Guglielmi, Y., Rutqvist, J., Tsang, C.-F. & Thoraval, A., 2008. Estimation of fracture flow parameters through numerical analysis of hydromechanical pressure pulses, *Water Resour. Res.,* **44,** W11408, doi:10.1029/2008WR007015.

Cardiff, M., Bakhos, T., Kitanidis, P. & Barrash, W., 2013. Aquifer heterogeneity characterization with oscillatory pumping: sensitivity analysis and imaging potential, *Water Resour. Res.,* **49,** 5395–5410.

Davis, E. & Becker, K., 2004. Observations of temperature and pressure: constraints on ocean crustal hydrologic state, properties, and flow, in *Hydrogeology of the Oceanic Lithosphere,* chap. 8, pp. 225–271, eds. Davis, E. & Elderfield, H., Cambridge Univ. Press.

Detournay, E. & Cheng, A.-D., 1995. Fundamentals of poroelasticity, in *Comprehensive Rock Engineering: Principles, Practice and Projects,* p. 752, ed. Brown, E.T., Pergamon.

do Nascimento, A., Lunn, R. & Cowie, P., 2005. Modeling the heterogeneous hydraulic properties of faults using constraints from reservoir-induced seismicity, *J. geophys. Res.,* **110,** 1–17.

Dow, T., Long, J., Endo, H. & Wilson, C., 1982. Approaches to evaluating the permeability and porosity of fractured rock masses, pp. 281–292, eds. Goodman, R. & Heuze, F., Soc. of Mining Eng. of the Am. Inst. of Mining.

Fetter, C., 2001. *Applied Hydrogeology,* Prentice Hall.

Fokker, P., Renner, J. & Verga, F., 2013. Numerical modeling of periodic pumping tests in wells penetrating a heterogeneous aquifer, *American Journal of Environmental Science,* **9,** 1–13.

Gellasch, C., Wang, H., Bradbury, K., Bahr, J. & Lande, L., 2014. Reverse water-level fluctuations associated with fracture connectivity, *Groundwater,* **52,** 105–117.

Gringarten, A., Ramey, H. & Raghavan, R., 1974. Unsteady-state pressure distributions created by a well with a single infinite-conductivity vertical fracture, *Society of Petroleum Engineers (August),* pp. 347–360, doi:10.2118/4051-PA.

Gringarten, A., Ramey, H. & Raghavan, R., 1975. Applied pressure analysis for fractured wells, *Journal of Petroleum Engineers,* **27,** SPE–5496–PA, doi:10.2118/5496-PA.

Guiltinan, E. & Becker, M., 2015. Measuring well hydraulic connectivity in fractured bedrock using periodic slug tests, *J. Hydrol.,* **521,** 100–107.

Jacob, C., 1940. On the flow of water in an elastic artesian aquifer, *Transactions, American Geophysical Union,* **21,** 574–586.

James, J. & Butler, J., 1997. *The Design, Performance, and Analysis of Slug Tests,* Development in water, CRC Press LLC.

Johnson, C., Greenkorn, R. & Woods, E., 1966. Pulse-testing: a new method for describing reservoir flow properties between wells, *J. Petrol. Tech.,* **18,** 1599–1604.

Kamal, M. & Brigham, W., 1975. Pulse-testing response for unequal pulse and shut-in periods, *Soc. Petrol. Eng. J.,* **15,** 399–410.

Krauss, I., 1974. Brunnen als seismische Übertragungssysteme, *PhD thesis,* Universität Frankfurt/Main.

Marschall, P. & Barczewski, B., 1989. The analysis of slug tests in the frequency domain, *Water Resour. Res.,* **25,** 2388–2396.

Matthews, C.S. & Russell, D.G., 1967. *Pressure buildup and flow tests in wells,* Monograph Series, Society of Petroleum Engineers.

Mavko, G., Mukerji, T. & Dvorkin, J., 2009. *The Rock Physics Handbook: Tools for Seismic Analysis of Porous Media,* Cambridge Univ. Press.

Moench, A., 1984. Double-porosity models for a fissured groundwater reservoir with fracture skin, *Water Resour. Res.,* **20,** 831–846.

Murdoch, L.C. & Germanovich, L.N., 2006. Analysis of a deformable fracture in permeable material, *Int. J. Numer. Anal. Methods Geomech.,* **30,** 529–561.

Murdoch, L.C. & Germanovich, L.N., 2012. Storage change in a flat-lying fracture during well tests, *Water Resour. Res.,* **48,** W12528, doi:10.1029/2011WR011571.

Narasimhan, T., 2006. On storage coefficient and vertical strain, *Groundwater,* **44,** 488–491.

Ortiz, A., Jung, R. & Renner, J., 2013. Two-dimensional numerical investigations on the termination of bilinear flow in fractures, *Solid Earth,* **4,** 331–345.

Ortiz, A.E., Renner, J. & Jung, R., 2011. Hydromechanical analyses of the hydraulic stimulation of borehole Basel 1, *Geophys. J. Int.,* **185,** 1266–1287.

Rasmussen, T., Haborak, K. & Young, M.H., 2003. Estimating aquifer hydraulic properties using sinusoidal pumping at the Savannah River sie, South Carolina, USA, *Hydrogeology Journal,* **11,** 466–482.

Renner, J. & Messar, M., 2006. Periodic pumping tests, *Geophys. J. Int.,* **167,** 479–493.

Renner, J. & Steeb, H., 2014. *Handbook of Geomathematics, Modeling of Fluid Transport in Geothermal Research,* 2nd edn 2015, eds. Freeden, W., Nashed, M. & Sonar, T., Springer, doi:10.1007/978-3-642-27793-1_81-2.

Russell, D. & Truitt, N., 1964. Transient pressure behavior in vertically fractured reservoirs, *J. Petrol. Tech.,* **16,** 1159–1170.

Schweisinger, T., Svenson, E. & Murdoch, L., 2009. Introduction to hydromechanical well tests in fractured rock aquifers, *Ground Water,* **47,** 69–79.

Shapiro, S.A. & Dinske, C., 2009. Scaling of seismicity induced by nonlinear fluid-rock interaction, *J. geophys. Res.,* **114,** B09307, doi:10.1029/2008JB006145.

Shapiro, S.A., Rentsch, S. & Rothert, E., 2005. Characterization of hydraulic properties of rocks using probability of fluid-induced microearthquakes, *Geophysics,* **70,** F27–F33.

Slack, T.S., Murdoch, L.C., Germanovich, L.N. & Hisz, D.B., 2013. Reverse water-level change during interference slug tests in fractured rock, *Water Resour. Res.,* **49,** 1552–1567.

Sneddon, I.N., 1995. *Fourier Transforms,* Dover Publications.

Stegemeier, G., 1982. Interwell pressure testing for field pilots, *SPE,* 11086, doi:10.2118/11086-MS.

Valkó, P. & Economides, M., 1995. *Hydraulic Fracture Mechanics,* John Wiley & Sons.

van Everdingen, A. & Meyer, L., 1971. Analysis of buildup curves obtained after well treatment, *Society of Petroleum Engineers,* SPE-2864, 513–524.

Vasco, D. & Minkoff, S., 2009. Modelling flow in a pressure-sensitive, heterogeneous medium, *Geophys. J. Int.,* **179,** 972–989.

Vinci, C., Renner, J. & Steeb, H., 2014a. A hybrid-dimensional approach for an efficient numerical modeling of the hydro-mechanics of fractures, *Water Resour. Res.,* **50,** 1616–1635.

Vinci, C., Renner, J. & Steeb, H., 2014b. On attenuation of seismic waves associated with flow in fractures, *Geophys. Res. Lett.,* **41,** 7515–7523.

Wang, H., 2000. *Theory of Linear Poroelasticity with Applications to Geomechanics and Hydrogeology,* Princeton University Press.

Weir, G.J., 1999. Single-phase flow regimes in a discrete fracture model, *Water Resour. Res.,* **35,** 65–73.

Wolff, R., 1970. Relationship between horizontal strain near a well and a reverse water level fluctuation, *Water Resour. Res.,* **6,** 1721–1728.